Anal. Chem. **2003,** *75,* 5797−5805

Critical Flocculation Concentrations, Binding Isotherms, and Ligand Exchange Properties of Peptide-Modified Gold Nanoparticles Studied by UV−Visible, Fluorescence, and Time-Correlated Single Photon Counting Spectroscopies

Huan Xie,[†] Alexander G. Tkachenko,[†] Wilhelm R. Glomm,[†] Joseph A. Ryan,[†] Matthew K. Brennaman,[‡] John M. Papanikolas,[‡] Stefan Franzen,*[,†] and Daniel L. Feldheim*[,†]

Department of Chemistry, North Carolina State University, Raleigh, North Carolina 27695, and Department of Chemistry, University of North Carolina, Chapel Hill, North Carolina 27599

Protocols for modifying gold nanoparticles with peptide−bovine serum albumin (BSA) conjugates are described within. The resulting constructs were characterized using a number of techniques including static fluorescence spectroscopy and time-correlated single photon counting spectroscopy (TCSPC) in order to quantify peptide−BSA binding isotherms, exchange rates, critical flocculation concentrations, and the composition of mixed peptide−BSA monolayers on gold nanoparticles. TCSPC has proven to be a powerful technique for observing the microenvironment of protein−gold nanoparticle conjugates because it can distinguish between surface-bound and solution-phase species without the need for separation steps. Full characterization of the composition and stability of peptide-modified metal nanoparticles is an important step in their use as intracellular delivery vectors and imaging agents.

This paper addresses fundamental issues involving the adsorption of peptide-modified protein conjugates onto gold nanoparticles. Metal particle bioconjugates are important constructs for cellular imaging, therapeutic delivery, and biomolecule detection.[1−4] For example, Schultz et al. used gold and silver particles as immunohistochemical staining reagents to selectively label regions of the *Drosophila* X chromosome.[3] Because of the remarkably large scattering cross section of metal particles (10^{-10} cm^2), individual nanoparticles can be imaged under white-light illumination. Moreover, the plasmon resonance condition of metals can be tuned across the visible spectrum and into the near-infrared simply by changing particle size and shape.[5−7] Thus, multicolor assays are possible with a single light source, without the need for filters, and free from complications of fluorescence bleaching or blinking.

We have employed gold particle bioconjugates to study cellular uptake of peptides and antibodies.[4] The constructs used in our studies are based on those described in the pioneering work of Feldherr et al.[2] In their work, cell-targeting peptides were conjugated to bovine serum albumin (BSA). The peptide−BSA conjugates were subsequently adsorbed onto gold nanoparticles, microinjected into a HeLa cell line and imaged with transmission electron microscopy.

A major goal of modern therapeutic delivery and tissue imaging is to create a bioconjugate capable of seeking out specific cells in vivo, traversing the cell and nuclear membranes, and releasing a therapeutic in the nucleus. Our work has sought to accomplish these tasks by combining multiple membrane-translocating peptides and antibodies onto a *single* gold nanoparticle. Of importance in this work is understanding how to formulate BSA−gold bioconjugates that are stable in high ionic strength solutions containing exchangeable peptides and proteins and how to quantify the number of adsorbed biomolecules per gold particle. This paper addresses these fundamental issues using a combination of classic and time-resolved fluorescence spectroscopy studies.

MATERIALS AND METHODS

Materials. Gold nanoparticles (20-nm diameter) were purchased from Ted Pella. BSA was purchased from Roche (MW, 67 000). 3-Maleimidobenzonic acid *N*-hydroxysuccinimide ester (MBS), dithiothreitol (DTT), rhodamine B isothiocyanate (RBITC), glutathione, lysine, fluorescamine, and 5,5′-dithio-bis(2-nitrobenzoic acid) (DTNB) were obtained from Sigma-Aldrich. Ruthenium(II) tris(2,2′-bipyridine)monohexanethiol ($[Ru(bipy)_2bipy\text{-}C_6H_{12}\text{-}SH]^{2+}$) was synthesized as described previously.[8−11]

Sephadex G10−50 was purchased from Sigma. Centricon YM-30 and Microcon YM-100 were purchased from Millipore. The

* To whom correspondence should be addressed. E-mail: Stefan_Franzen@NCSU.edu; Dan_Feldheim@NCSU.edu.

[†] North Carolina State University.

[‡] University of North Carolina.

(1) Cao, Y.; Jin, R.; Mirkin, C. A. *J. Am. Chem. Soc.* **2001**, *123*, 7961−7962.

(2) Feldherr, C. M.; Lanford, R. E.; Akin, D. *Proc. Natl. Acad. Sci. U.S.A.* **1992**, *89*, 11002−11005.

(3) Schultz, S.; Smith, D. R.; Mock, J. J.; Schultz, D. A. *Proc. Natl. Acad. Sci. U.S.A.* **2000**, *97*, 996−1001.

(4) Tkachenko, A. G.; Xie, H.; Coleman, D.; Glomm, W.; Ryan, J.; Anderson, M. F.; Franzen, S.; Feldheim, D. L. *J. Am. Chem. Soc.* **2003**, *125*, 4700−4701.

(5) Haes, A.; Van Duyne, R. *J. Am. Chem. Soc.* **2002**, *124*, 10596−10604.

(6) West, J. L.; Halas, N. J. *Curr. Opin. Biotechnol.* **2000**, *11*, 215−217.

(7) Jin, R.; Cao, Y.; Mirkin, C. A.; Kelly, K.; Schatz, G.; Zheng, J. *Science* **2001**, *294*, 1901−1903.

10.1021/ac034578d CCC: $25.00
Published on Web 09/30/2003

Table 1. Peptides Used for Assembling Gold Particle−Peptide Conjugates

no.	peptide sequence	origin of peptide	MW	pK_I
I	CGGFSTSLRARKA	adenoviral NLS	1353	12.3
II	CKKKKKKSEDEYPYVPN	adenoviral RME	2084	9.3

7.5% Tris-HCl prepacked PAGE gels and protein assay kit were purchased from Bio-Rad.

All UV−visible absorption measurements were acquired on a Hewlett-Packard 8453 Chemstation photodiode array spectrophotometer with attached Chemstation software. Emission spectra were acquired using an RF-5301 PC spectrofluorophotometer or PTI Quantamaster luminescence spectrometer (MD-5020). Quantification of $[Ru(bipy)_2bipy\text{-}C_6H_{12}\text{-}S]^{2+}$-labeled BSA on gold nanoparticles was performed by time-correlated single photon counting (TCSPC). Ellman and fluorescamine analyses were performed on BioTek FL-600 plate reader.

The two peptide sequences investigated in this work (Table 1) were synthesized by The University of North Carolina Peptide Synthesis Facility.

Preparation of BSA−MBS−Peptide Conjugates. BSA was conjugated to peptides by coupling the bifunctional linker MBS to BSA. For example, MBS was dissolved in dimethylformamide (10 mg/mL) and added to aqueous solutions containing BSA (10 mg/mL, in pH 7.2 PBS buffer) to produce a molar ratio of MBS to BSA of 40:1. The reaction was allowed to proceed for 30 min at room temperature. Sephadex G-50 was employed to remove unreacted MBS. In a separate reaction flask, DTT (10 mg) was added to an aqueous solution containing peptide I or II (5 mg/mL in pH 7.4 PB buffer) and the resultant mixture stirred for 1 h at room temperature. Excess DTT was separated by gel filtration on a G10 column. BSA−MBS conjugates were then mixed with the peptide solution (20:1 peptide/BSA ratio) and stirred for 5 h. Free peptides were removed from the mixture by centrifugal solvent displacement (Centricon YM-30 at 5000 rpm). Similar protocols were used to prepare fluorescently labeled BSA, with the exception that rhodamine B isothiocyanate (RB) was reacted directly with BSA without the use of MBS at 4 °C for 12 h.

Determination of BSA-Bound MBS Using Fluorescamine. MBS binds to the lysine residues of BSA to form BSA−MBS conjugates. The number of free lysine residues on BSA should decrease with increasing amounts of added MBS. The nonfluorescent compound fluorescamine (4-phenylspiro[furan-2(3*H*)-1′-phthalan]-3,3′-dione) reacts rapidly with primary amines in proteins, such as the terminal amino group of peptides and the ϵ-amino group of lysine, to form highly fluorescent pyrrolinone moieties.[12] This reaction was employed to determine the number of lysines per BSA that reacted with MBS, as a function of MBS added to the reaction mixture.

MBS−BSA binding isotherms were generated by preparing MBS−BSA conjugates with various ratios of added MBS (10:1−135:1 MBS/BSA). The resulting conjugates were purified from excess MBS and reacted with 250 μM fluorescamine at pH 7.4 in flat-bottom low-fluorescence 96-well plates. Sample fluorescence was measured using a BioTek FL-600 plate reader with 360 ± 40 (EX) and 460 ± 40 nm (EM) filters.

Determination of BSA−MBS Bound Sulfhydryl Using DTNB (Ellman's Reagent). Ellman's test for thiols was used as a second quantitative method of the MBS−BSA conjugation reaction.[13] MBS−BSA conjugates with various ratios of added MBS (10:1−135:1 MBS/BSA) were prepared. After unreacted MBS was removed, BSA-MBS complexes were combined with β-mercaptoethanol (BME) or glutathione (GSH) in V-bottom 96-well plates at the following ratios of BSA/MBS/thiol: 1:10, 1:20, 1:40, 1:60, and 1:80 in 50 mM phosphate buffer (pH 7.4) and 50 mM EDTA. After 4 h of reaction, 45-μL aliquots of the reaction were transferred to flat-bottom 96-well plates and reacted with 50 μM DTNB in 50 mM Tris·HCl pH 8.2 and 50 mM EDTA. After 15 min, visible light absorption was measured at 405 nm using a BioTek FL-600 plate reader to determine the amount of unbound BME and GSH. The difference of total thiol added and unbound thiol yielded the number of bound thiols per BSA.

Preparation of BSA−MBS−$[Ru(bipy)_2bipy\text{-}C_6H_{12}\text{-}SH]^{2+}$ Conjugates. A solution of $[Ru(bipy)_2bipy\text{-}C_6H_{12}\text{-}SH]^{2+}$ (1 mM) was added to 1-mL aliquots of BSA/MBS (1 mg/mL) to yield an initial molar ratio of 15:1 $[Ru(bipy)_2bipy\text{-}C_6H_{12}\text{-}SH]^{2+}$ per BSA−MBS and allowed to mix for 60 min. All samples were then separated from excess $[Ru(bipy)_2bipy\text{-}C_6H_{12}\text{-}SH]^{2+}$ by centrifugal filtration (Centricon, YM- 30). Steady-state emission spectra were recorded on a PTI Quantamaster luminescence spectrometer (MD-5020) using 450-nm excitation while monitoring emission intensity from 530 to 700 nm. The emission quantum yield of the C_6H_{12}-SH-modified $[Ru(bpy)_3]^{2+}$ was determined using a luminescent compound with a known quantum yield; $[Ru(bpy)_3]^{2+}$ (QY = 0.042 ± 0.002 at 25 °C[14]). Absorbance (UV−visible) and steady-state emission spectra were collected for aqueous solutions containing either modified or unmodified $[Ru(bpy)_3]^{2+}$. By comparing the steady-state emission peak areas for solutions containing identical concentrations of modified and unmodified $[Ru(bpy)_3]^{2+}$, the ratio of the quantum yields was found. The quantum yield of $[Ru(bpy)_2bpy\text{-}C_6H_{12}\text{-}SH]^{2+}$ was calculated to be 0.026 ± 0.003 at 25 °C.

Flocculation Assays and Critical Flocculation Concentration (CFC) Tests. Flocculation assays were performed to determine the approximate amount of biomolecules required to stabilize gold nanoparticles. In a typical assay involving peptide−BSA conjugates, gold sol was adjusted to pH 9 with 50 mM carbonate buffer. A 0.7-mL aliquot of gold sol (1.05 nM) was added to six vials containing 100 μL of BSA−peptide conjugate with concentrations ranging from 0.22 to 1.83 μM. After 5 min, 80 μL of 10% NaCl solution was added to the sols to test for flocculation. The CFC tests were done by sequential addition of electrolytes (1.5 M NaCl as described above) to aqueous suspensions of the conjugates. CFC was determined as the concentration of electrolyte at which the gold particle plasmon absorption shifted from its characteristic maximum of 526 nm to ~600 nm. Similar methods were used in flocculation assays involving native BSA, with the exception that the assays were performed in pH 7

(8) Sato, Y.; Uosaki, K. *J. Electroanal. Chem.* **1995**, *384*, 57−66.
(9) Yamada, S.; Koide, Y.; Matsuo, T. *J. Electroanal. Chem.* **1997**, *426*, 23−26.
(10) Dellaciana, L.; Hamachi, I.; Meyer, T. J. *J. Org. Chem.* **1989**, *54*, 1731−1735.
(11) Maier, V. E.; Shafirovich, V. Y. *B Acad. Sci. USSR Ch+* **1989**, *38*, 626−628.
(12) Udenfrie, S.; Stein, S.; Bohlen, P.; Dairman, W. *Science* **1972**, *178*, 871−872.
(13) Ellman, G. L. *Arch. Biochem. Biophys.* **1959**, *82*, 70−77.
(14) Vanhouten, J.; Watts, R. J. *J. Am. Chem. Soc.* **1976**, *98*, 4853−4858.

phosphate buffer and the gold sol was added to six vials containing 100 μL of BSA with concentrations ranging from 1.85 to 5.85 μM.

Quantifying [Ru(bipy)$_2$bipy-C$_6$H$_{12}$-S]$^{2+}$-Labeled BSA on Gold Nanoparticles by Time-Correlated Single Photon Counting. The surface coverage of [Ru(bipy)$_2$bipy-C$_6$H$_{12}$-S]$^{2+}$-labeled BSA on 20-nm gold colloids was determined using TCSPC. Transients were obtained for the pure [Ru(bipy)$_2$bipy-C$_6$H$_{12}$-S]$^{2+}$-labeled BSA solution (1 mg/mL; preparation described above) and for a solution with 20-nm gold colloids mixed with a ratio of 500:1 [Ru(bipy)$_2$bipy-C$_6$H$_{12}$-S]$^{2+}$-labeled BSA/gold.

Time-Resolved Emission Methods. Time-resolved emission spectra were acquired with an argon ion laser whose continuous output was used to pump a mode-locked Ti:sapphire oscillator. The Ti:sapphire laser output was frequency doubled to 423 nm using a BBO crystal to produce ~1-ps pulses with a pulse energy of ~ 0.26 nJ/pulse. This pulse train was pulse picked and the repetition rate selected to be roughly 5 times the natural lifetime of the sample. Luminescence lifetime data were collected using the time-correlated single photon counting technique published earlier.[15] Samples were sparged with argon for ~45 min prior to use.

The method for analysis of the fraction of luminescent molecules on the surface of a nanoparticle and in solution has been also published previously.[15] Relaxation from the radiative excited states was modeled using the following exponential decays:

$$Y(t) = \sum_{i=1}^{N} A_i e^{-k_i t} \quad (1)$$

where N is the total number of phosphorescent components and A_i and k_i represent the amplitude is rate constant for each component, respectively. The final fit was approached using an iterative process where exponentials were added until no significant improvements in the correlation coefficient of the fit could be seen. The calculated populations associated with each observed lifetime were then compared to the initial added concentration of emitter (free in solution) in order to determine the number of emitters associated with the gold colloids. For example, if there are two populations, there will be two observed lifetimes. The radiative rate constant for unquenched Ru(bipy)$_3^{2+}$ in solution is

$$1/\tau_{obs} = 1/\tau_{phos} + 1/\tau_{non-rad} \quad (2)$$

where $k_{obs} = 1/\tau_{obs}$, $k_{phos} = 1/\tau_{phos}$, etc. The phosphorescence lifetime is τ_{obs}, and the nonradiative lifetime is $\tau_{non-rad}$. Quenching can occur by electron or energy transfer from [Ru(bipy)$_2$bipy-C$_6$H$_{12}$-S]$^{2+}$ to the gold nanoparticle with rate constant, k_{et} to give an observed lifetime of

$$1/\tau_{obs} = 1/\tau_{phos} + 1/\tau_{non-rad} + 1/\tau_{et} \quad (3)$$

The phosphorescence quantum yield is

$$\phi = k_{phos}/(k_{phos} + k_{non-rad} + k_{et}) \quad (4)$$

where $k_{et} = 0$ for the solution fraction. It turns out that the ratio of the amplitudes, A_i/A_j in the fit correspond exactly to the ratio of the amounts of [Ru(bipy)$_2$bipy-C$_6$H$_{12}$-S]$^{2+}$ in phases i and j, respectively.[16]

Quantifying Fluorescently Labeled BSA or BSA−Peptide Conjugates on Gold Nanoparticles by Fluorescence Spectroscopy. BSA coverage on 20-nm-diameter gold particles was determined with fluorescence spectroscopy. In a typical experimental procedure (e.g., to generate a binding isotherm plot), BSA was labeled with rhodamine B isothiocyanate (RB−BSA) and purified by centrifugal solvent displacement (Centricon YM-30 at 5000 rpm). The concentration of RB−BSA following purification was determined with a protein assay (Bio-Rad DC protein assay), and standard curves of fluorescence versus RB−BSA concentration were measured. RB−BSA solutions were prepared at concentrations (nine solutions of 30 μL each) ranging from 0.39 to 11.7 μM. Gold nanoparticles (450 μL of 1.05 μM solution) in aqueous phosphate solution buffered at pH 7.0 were added to each RB−BSA solution. After stirring for 15 min, 20 μL of 2 mg/mL native BSA (e.g., unlabeled BSA) was added to each solution.[17,18] Native BSA was required in order to block open gold particle surface sites and prevent flocculation. That is, the RB−BSA concentrations corresponding to submonolayer coverage resulted in particles that were unstable toward flocculation. Experiments in which the exchange of RB−BSA for native BSA was monitored in time revealed this to be a slow process (hours). Thus, within the time scale of the RB−BSA adsorption isotherm experiments, bound RB−BSA was not displaced by the native BSA stabilizer. Following addition of RB−BSA to gold nanoparticle sols, we sought to measure the unbound fraction of RB−BSA. To remove the unbound fraction, the nanoparticle sols were centrifuged by Microcon at 2.6×10^3 rpm for 15 min. The sediment was washed three times with 50 μL of 50 mM pH 7.0 phosphate buffer. The final sediment was transferred to a new vial, centrifuged at 3.3×10^3 rpm for 8 min, and resuspended in buffer. The aliquots of supernatant were diluted to 2 mL, and fluorescence of the supernatant was measured and compared to the standard curve to determine the concentration of unbound RB−BSA in the initial mixture. The amount of RB−BSA bound to the gold particles was calculated by subtracting free RB−BSA from the total amount of RB−BSA added initially. The number of gold nanoparticles in the sol was determined by UV−visible spectroscopy. Any loss from nonspecific adsorption of RB−BSA onto the Microcon was not taken into account.

Adsorption isotherms for peptide−BSA conjugates were determined by conjugating peptide I or II to RB−BSA via an MBS cross-linker. Gel electrophoresis was used to quantify the peptide/BSA ratio. Peptide−BSA−gold conjugates were assembled using the conditions reported for BSA−gold conjugates, with the exception that the gold sol was buffered with pH 9.0 carbonate buffer.

Quantifying Mixed BSA Adlayers. To determine the mole fraction of BSA−peptide I and BSA−peptide II conjugates bound to nanoparticles versus their mole fraction in a solution mixture,

(15) Brennaman, M. K.; Alstrum-Acevedo, J. H.; Fleming, C. N.; Jang, P.; Meyer, T. J.; Papanikolas, J. M. *J. Am. Chem. Soc.* **2002**, *124*, 15094−15098.
(16) Glomm, W. R.; Moses, S. J.; Brennaman, M. K.; Papanikolas, J. M.; Franzen, S. *J. Phys. Chem.*, submitted.
(17) Deroe, C.; Courtoy, P. J.; Baudhuin, P. *J. Histochem. Cytochem.* **1987**, *35*, 1191−1198.
(18) Horisberger, M.; Clerc, M. F. *Histochemistry* **1985**, *82*, 219−223.

BSA−peptide II conjugates were labeled with rhodamine B, while BSA−peptide I was kept unlabeled. Solution mixtures of BSA−peptide I and RB−BSA−peptide II conjugates were prepared with $X_{\text{peptide II}}$ of 1, 0.8, 0.6, 0.4, and 0.2, keeping the total amount of BSA constant. The amount of bound RB−BSA−peptide II per nanoparticle was determined using the procedures described above for single-component solutions. The amount of BSA−peptide I per nanoparticle was computed by subtracting the number of RB−BSA-peptide II per nanoparticle for $X_{\text{peptide II}} \neq 1$ from $X_{\text{peptide II}} = 1$.

BSA Exchange Studies. Three identical solutions of RB−BSA−gold complexes were prepared (1.05 nM). Glutathione (10 μL of 65.0 mM) was added to each aliquot of the first solution, native BSA (10 μL of 74.6 μM) was added to each aliquot of the second solution, and phosphate buffer (10 μL of 50 mM) was added to each aliquot of the third solution as a control. All aliquots were centrifuged and resuspended to separate bound and unbound BSA. The emission spectra of each supernatant were compared over time (20−240 min) to determine the rate of exchange of particle-bound RB−BSA in the presence of glutathione and native BSA.

RESULTS

BSA−MBS Conjugates. MBS is a heterobifunctional cross-linker with an NHS ester on one end and a maleimide group on the other. The NHS ester reacts with primary amines in BSA to form amide bonds, while the maleimide reacts with sulfhydryl groups to form thiol linkages.[19,20] The pH of the solution was kept in the range between 6.6 and 7.4 to promote attack of the maleimide by the thiol. At higher pH values, amines could potentially compete with the thiol for the maleimide binding sites, thus lowering the yield of thiol (RSH, where R = peptide or [Ru(bipy)$_3$]$^{2+}$) conjugation to the protein. Our first task in the construction of peptide−BSA−gold nanoparticle complexes was thus to determine the yield of MBS conjugation to BSA under varying reaction stoichiometry.

BSA contains 59 lysines out of which up to 35 were thought to reside on the surface and could potentially be used for maleimide modification (vide infra). The number of MBS ligands bound to BSA was determined experimentally by a fluorescent assay using fluorescamine.[12] Free fluorescamine does not fluoresce, but when reacted with amines, the resulting product has a strong emission at 460 nm. Thus, the number of MBS ligands conjugated to BSA can be quantified by determining the number of unreacted lysines and subtracting this value from the number of total reactive lysines on BSA (e.g., the number determined by performing a fluorescamine assay on BSA not exposed to MBS). This assay requires calibration of fluorescamine emission for a compound similar in chemical form to that produced when fluorescamine reacts with BSA. Two calibration standards were explored in this work: lysine monomer and (lysine)$_{16}$. Lysine monomers contain two potentially reactive amines; however, the yield of the reaction between fluorescamine and the N-terminal amine was unknown and could not be assumed as 100%. To measure the contribution of the N-terminus to the fluorescence from the lysine−fluorescamine standard curve, a calibration plot was generated using cysteine. Cysteine contains only the N-terminal amine, and as shown in Figure 1, the fluorescence resulting from the cysteine reaction is much less than that from the ϵ-amine of lysine. The difference in the lysine and cysteine calibration plots represents the fluorescence contribution from the ϵ-amine of lysine. This curve was used as a standard fluorescence curve for determining the number of lysines on BSA. To check the validity of this calibration standard, (lysine)$_{16}$ was also used to generate a standard curve. The fluorescence contribution from the N-terminus was assumed negligible compared to the other 16 amines of the polymer. Indeed, the calibration plot for (lysine)$_{16}$ was close to that generated by the lysine−cysteine difference method (Figure 1).

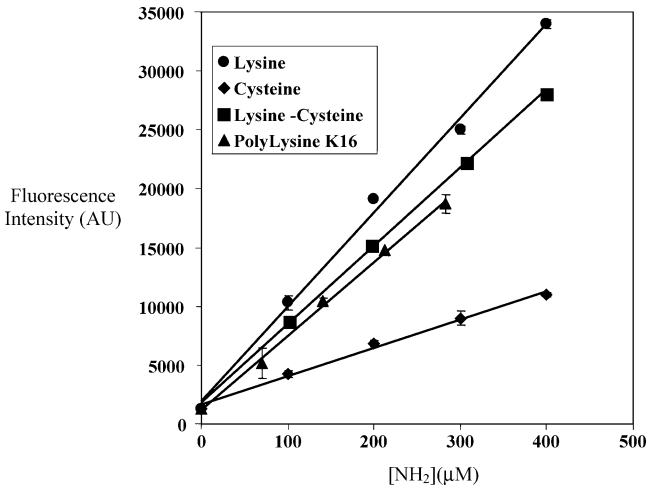

Figure 1. Standard curves for the reaction of fluorescamine and peptides. Fluorescence intensity is plotted vs total amine concentration for lysine and cysteine monomers and (lysine)$_{16}$. The plot of lysine−cysteine, and (lysine)$_{16}$ reveals the contribution of fluorescence from the ϵ-terminal amine of lysine.

Fluorescamine assays performed on native BSA determined that there are a total of 49 ± 7 lysines/BSA that are accessible to the fluorescamine reaction. The assay was used subsequently to determine the number of lysines on BSA following MBS coupling. A nonlinear decrease in the number of available lysine residues was observed, leveling out at a value corresponding to 34 ± 3 MBS linkers/BSA (Figure 2). These results agree well with prior reports, where out of the 59 lysines of BSA, only up to ~35 residues were reactive toward the NHS ester of MBS.[20]

The second step in the synthesis of peptide−BSA conjugates is reaction of sulfhydryl groups with MBS/BSA. While the fluorescamine assay can determine the number of MBS linkers reacted with the lysine residues of BSA, it cannot determine the number of maleimides subsequently conjugated to sulfhydryl groups, and it cannot be assumed that all of the MBS linkers tethered to BSA will react. Hydrolysis of maleimide in solution and steric constraints on the incoming sulfhydryl are two mechanisms that may prevent complete reaction. We thus sought to determine the number of maleimides available for functionalization with sulfhydryl groups on BSA. This was accomplished using Ellman analysis.[13] Ellman's reagent (DTNB) readily forms a mixed disulfide with thiols, liberating the chromophore 5-mercapto-2-nitrobenzoic acid (absorption maximum 410 nm, ϵ ~13 600 cm^{-1} M^{-1}). Since Ellman's reagent cannot determine the number of bound sufhydryls directly, the amount of unreacted thiol was

(19) Lanford, R. E.; Kanda, P.; Kennedy, R. C. *Cell* **1986**, *46*, 575−582.
(20) Hermanson, G. T. *Bioconjugate Techniques*; Academic Press: San Diego, 1996.

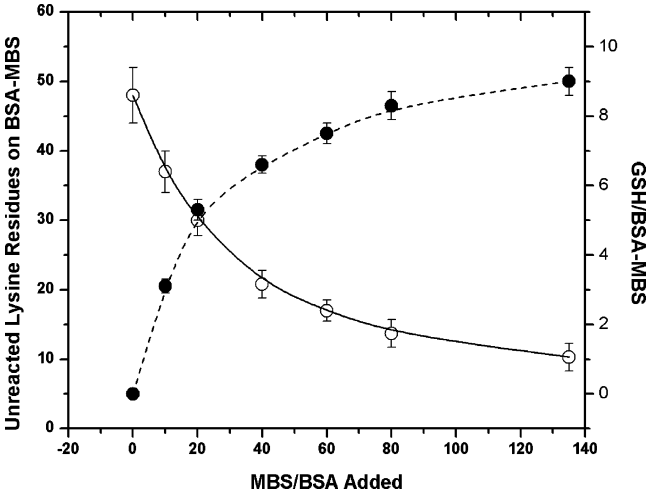

Figure 2. Number of MBS and GSH ligands conjugated to BSA. MBS binding is shown as a decrease of available lysine residues on BSA as determined by the fluorescamine assay (open circles, solid line). GSH binding is shown as the difference between added and unreacted GSH determined with Ellman's reagent (shaded circles, dashed line). (Lines are presented merely as guides.)

measured. GSH and BME were used as sources of thiol groups. Results for both thiols were essentially identical and showed 8.6 ± 1.2 thiol groups attached per BSA (Figure 2). This number was lower than expected since over 30 MBS ligands were attached to BSA.

Yield for Binding of $[Ru(bipy)_2bipy\text{-}C_6H_{12}\text{-}SH]^{2+}$ to BSA. The number of $[Ru(bipy)_2bipy\text{-}C_6H_{12}\text{-}SH]^{2+}$ labels attached to BSA was determined by comparing the emission of the BSA−$[Ru(bipy)_2bipy\text{-}C_6H_{12}\text{-}SH]^{2+}$ conjugate to that of a free $[Ru(bipy)_2bipy\text{-}C_6H_{12}\text{-}SH]^{2+}$ standard curve. After comparison of sample emissions to the standard curve, it was determined that there were 8 ± 1 $[Ru(bipy)_2bipy\text{-}C_6H_{12}\text{-}SH]^{2+}$ molecules/BSA under conditions where ~20 MBS molecules were conjugated to BSA. The yield for reaction of $[Ru(bipy)_2bipy\text{-}C_6H_{12}\text{-}SH]^{2+}$ with MBS was ~0.5 under the conditions studied here.

Flocculation Assays and CFC Test. Gold nanoparticle sols are unstable with respect to precipitation and will flocculate rapidly upon addition of electrolytes (NaCl, KI, etc).[21] Citrate-capped gold nanoparticles can be stabilized against flocculation by the addition of proteins such as BSA. Flocculation measurements were performed in order to investigate the stability of the constructs studied here in an environment similar to those applicable for biological systems. The number of proteins per gold nanoparticle required to stabilize a sol in electrolyte solution can be determined by monitoring solution absorbance at 526 nm versus BSA concentration. Figure 3 shows flocculation data for increasing concentrations of native BSA (Figure 3a) and BSA−peptide I (Figure 3b). The number of protein conjugates required per nanoparticle to form a stable sol in 0.155 M sodium chloride were 550 and 150, respectively.

Critical flocculation concentration (CFC) measurements were also employed to investigate the stability of the colloidal solutions under conditions of increased ionic strength. CFC measurements were performed on particles stabilized with a monolayer of protein (purified by centrifugation) and in the presence of excess protein (unpurified). Table 2 shows the order of stability of proteins on gold particles to follow:

BSA−peptide II > BSA−peptide I > BSA > citrate

Adsorption of $[Ru(bipy)_2bipy\text{-}C_6H_{12}\text{-}S]^{2+}$−BSA on 20-nm Gold Nanoparticles Studied by Visible Absorption Spectroscopy. The absorption spectrum of $[Ru(bipy)_2bipy\text{-}C_6H_{12}\text{-}S]^{2+}$-labeled BSA adsorbed onto 20-nm trisodium citrate-stabilized gold nanoparticles is nearly equal to the sum of the individual spectra of the components $(Ru(bipy)_2bipy\text{-}C_6H_{12}\text{-}SH^{2+}$ + BSA + 20-nm gold) (not shown). The spectrum shows an intense band centered at 527 nm, which corresponds to the Fröhlich frequency of 20-nm gold, as well as an additional band centered around 280−290 nm from the $[Ru(bipy)_2bipy\text{-}C_6H_{12}\text{-}SH]^{2+}$ and BSA contributions. From comparison with the monomer spectrum, it is also possible to see the metal-to-ligand charge-transfer $[Ru(bipy)_2bipy\text{-}C_6H_{12}\text{-}SH]^{2+}$ band centered at 450 nm even when the $[Ru(bipy)_2bipy\text{-}C_6H_{12}\text{-}S]^{2+}$−BSA is adsorbed onto gold nanoparticles. Upon protein adsorption, the shape of the gold plasmon band appears slightly red-shifted but is stable over time. This suggests that $[Ru(bipy)_2bipy\text{-}C_6H_{12}\text{-}S]^{2+}$−BSA is associated with the gold nanoparticles but has not caused extensive particle aggregation.

Adsorption of $[Ru(bipy)_2bipy\text{-}C_6H_{12}\text{-}S]^{2+}$−BSA on 20-nm Gold Nanoparticles Studied by Time-Correlated Single Photon Counting. Time-correlated single photon counting was used to determine the number of $[Ru(bipy)_2bipy\text{-}C_6H_{12}\text{-}S]^{2+}$−BSA molecules adsorbed to the surface of the gold particle. This technique is well-suited for this application because gold-bound $[Ru(bipy)_2bipy\text{-}C_6H_{12}\text{-}S]^{2+}$−BSA moieties exhibit a quenched emission lifetime compared to free $[Ru(bipy)_2bipy\text{-}C_6H_{12}\text{-}S]^{2+}$−BSA in solution. Figure 4 shows time-resolved emission of $[Ru(bipy)_2bipy\text{-}C_6H_{12}\text{-}S]^{2+}$−BSA (0.2 μM) and $[Ru(bipy)_2bipy\text{-}C_6H_{12}\text{-}S]^{2+}$−BSA adsorbed to 20-nm gold nanoparticles (concentrations of 0.2 μM and 0.4 nM, respectively, corresponding to a $[Ru(bipy)_2bipy\text{-}C_6H_{12}\text{-}S]^{2+}$−BSA−gold molar ratio of 500:1). $[Ru(bipy)_2bipy\text{-}C_6H_{12}\text{-}S]^{2+}$−BSA decays with single-exponential kinetics and an observed lifetime of 1.5 μs. The mixed protein−gold transient was best fit to a biphasic model, with observed lifetimes of 1.8 μs and 14 ns, respectively. Table 3 shows the observed lifetimes of the systems investigated herein, as well as their relative populations.

Adsorption Isotherms for BSA on Gold Nanoparticles. Flocculation assays provide a rough estimate of the number of proteins required to stabilize a sol in solutions of high ionic strength. They do not, however, indicate the number of proteins bound per gold particle, nor do they provide information on the strength of protein adsorption. Adsorption isotherms—plots of the number of proteins adsorbed versus protein concentration—were thus generated in order to estimate K_d and saturation coverages for RB−BSA and BSA−peptide conjugates. A difference measurement in which the RB−BSA concentration remaining in solution was measured and subtracted from the starting concentration was necessary to quantify the number of BSA proteins per gold nanoparticle because RB−BSA emission is quenched on gold.

Adsorption isotherms for BSA conjugates are shown in Figure 5. Formally, adsorption isotherms are only valid for systems in equilibrium. Three experiments are suggestive of equilibrium adsorption in the systems studied here: (i) the amount of BSA

(21) Keating, C. D.; Musick, M. D.; Keefe, M. H.; Natan, M. J. *J. Chem. Educ.* **1999**, *76*, 949−955.

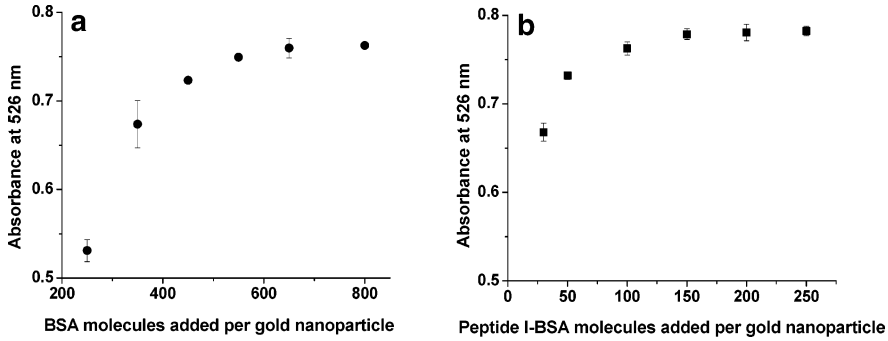

Figure 3. Absorbance at 526 nm for aqueous solutions containing BSA−gold nanoparticle conjugates and NaCl (0.17 M). (a) Absorbance vs added number of BSA molecules per Au particle. (b) Absorbance at 526 nm vs added number of BSA−peptide I molecules per Au particle. Spectra were taken 1 h after addition of NaCl. Error bars represent the deviation from three experiments. (In some experiments, the error was smaller than the data point.)

Table 2. Critical Flocculation Concentrations (CFC) for 20-nm Au Colloids with Various Stabilizing Agents[a]

solutions	CFC_{UC} (M)	CFC_C (M)
citrate Au	<0.033	0.012 ± 0.002
Au/BSA (1:200)	0.048 ± 0.006	0.301 ± 0.006
Au/BSA (1:1000)	0.53 ± 0.02	0.078 ± 0.003
Au/BSA (1:2000)	>1.0	0.085 ± 0.010
Au/BSA−peptide I (1:1000)	>1.0	0.130 ± 0.008
Au/BSA−peptide II (1:1000)	>1.0	>1.0

[a] Flocculent was 1.7 M NaCl. The numbers in parentheses represent the molar ratio of gold colloid to (added) adsorbate. The subscripts "UC" and "C" refer to uncentrifuged and centrifuged samples, respectively, where centrifuged samples were those centrifuged to remove excess stabilizer.

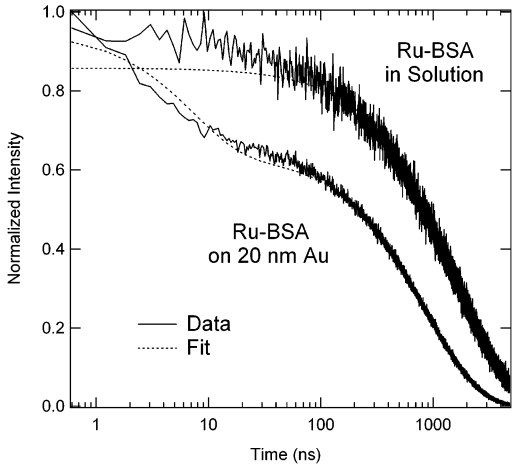

Figure 4. Normalized intensity versus time for solutions of [Ru(bipy)$_2$bipy-C_6H_{12}-S]$^{2+}$−BSA in solution and [Ru(bipy)$_2$bipy-C_6H_{12}-S]$^{2+}$−BSA + 20 nm Au colloids. The concentration of [Ru(bipy)$_2$bipy-C_6H_{12}-S]$^{2+}$−BSA was 0.2 μM in solution, and the 20-nm Au colloid concentration was 0.4 nM. The data are shown as solid lines and the fits as dashed lines.

adsorbed per particle did not change over the course of several hours, (ii) fluorescently labeled BSA in solution exchanged native BSA bound to gold nanoparticles (vide infra), and (iii) BSA desorbed, albeit slowly, over time when placed in neat aqueous solution. Nonlinear regression was applied to analyze the RB−BSA saturation curve. A one-site, Langmuir isotherm binding model yielded a K_d of 100 nM and a saturation coverage of 160 RB−BSA/gold nanoparticle.

In contrast to RB−BSA, the isotherm for BSA−peptide I conjugates revealed a linear regime with a small plateau region near 80 proteins/nanoparticle. BSA−peptide II conjugate gave a similar linear binding isotherm with a plateau at ∼ 150 molecules/particle.

Quantifying Mixed BSA Adlayers on Gold Nanoparticles. A primary motivation for using gold nanoparticles as vectors for therapeutic delivery is the potential to attach multiple membrane-targeting peptides, antibodies, and therapeutics to a single particle. The benefits of this strategy were illustrated recently with nanoparticles carrying separate peptides (as the BSA conjugate) for triggering receptor-mediated endocytosis and nuclear translocation in HepG2 cell lines.[4] Particles carrying either BSA−peptide conjugate alone were incapable of nuclear localization, but particles carrying both peptides showed efficient nuclear uptake. A major concern in the assembly of multi-peptide cell targeting vectors is whether the ratio of peptides bound to the particle reflects that originally added to solution. As Figure 6 shows, the mole fraction of BSA−peptide conjugates bound to nanoparticles nearly reflects the mole fraction of the two types of biomolecules added to solution. The difference in $X_{particle}$ versus $X_{solution}$ likely reflects a difference in K_d between the two BSA−peptide conjugates.

BSA Exchange. The tripeptide glutathione (γ-Glu-Cys-Gly) is a highly abundant component of living cells[22] Previous research has shown that glutathione forms a compact monolayer on polycrystalline gold surfaces, retaining its nonsulfhydryl biological activity.[23,24] Since one of our applications of gold−biomolecule complexes is delivery into cells, it is essential to know whether glutathione replaces biomolecules on the gold nanoparticle surface. To investigate exchange, a solution containing RB−BSA-coated gold nanoparticles was divided in three. Glutathione (10 μL of 65.0 mM) was added to one vial, native BSA to the second (10 μL of 74.6 μM), and 10 μL of phosphate buffer to the third vial as control. If glutathione exchanges RB−BSA, supernatants of the vial containing glutathione should have higher fluorescence intensities than those samples without glutathione. However, experiments showed no difference in fluorescence intensities of

(22) Stryer, L. *Biochemistry*, 4th ed.; W. H. Freeman and Co.: New York, 1995.
(23) Schaaff, T. G.; Knight, G.; Shafigullin, M. N.; Borkman, R. F.; Whetten, R. L. *J. Phys. Chem. B* **1998**, *102*, 10643−10646.
(24) Alvarez, M. M.; Khoury, J. T.; Schaaff, T. G.; Shafigullin, M. N.; Vezmar, I.; Whetten, R. L. *Chem. Phys. Lett.* **1997**, *266*, 91−98.

Table 3. Lifetimes and Calculated Populations[a]

system	lifetime τ_{obs}, ns	relative population	lifetime designation[a]
$[Ru(bipy)_2bipy\text{-}C_6H_{12}\text{-}SH]^{2+}$	1366.6	0.95	solution
$[Ru(bipy)_2bipy\text{-}C_6H_{12}\text{-}SH]^{2+}$-BSA	1496.4	0.92	solution
$[Ru(bipy)_2bipy\text{-}C_6H_{12}\text{-}SH]^{2+}$-BSA + 20-nm citrate gold	14.4 1785.8	0.31 0.63	surface solution

[a] Refers to the classification of an adsorbate and its relative population as either surface-confined or free in solution.

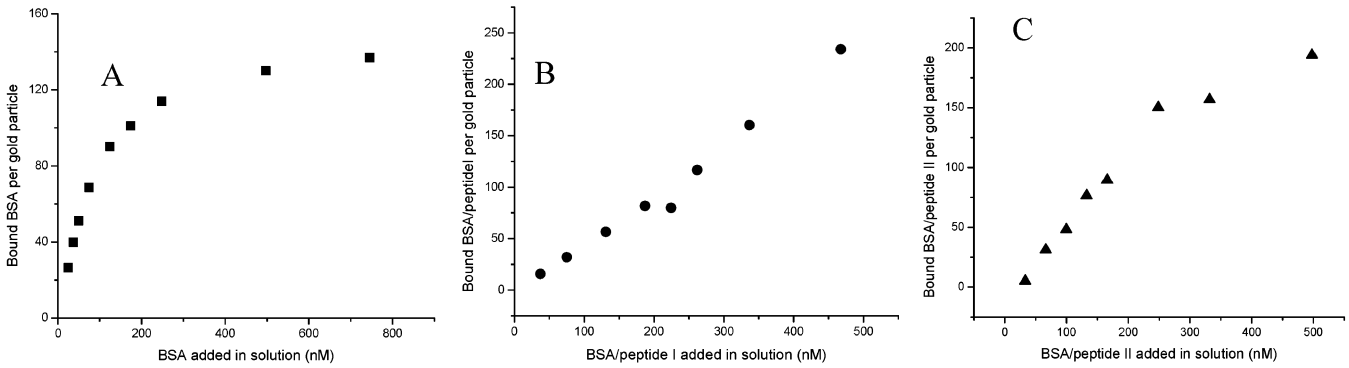

Figure 5. Adsorption isotherms of RBITC-labeled BSA (A), RBITC-labeled BSA−peptide I (B) and RBITC-labeled BSA−peptide II (C) adsorbed on gold particles (20 nm in diameter).

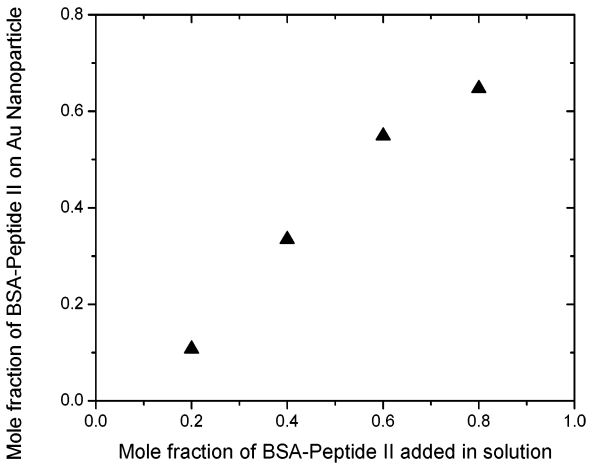

Figure 6. Mole fraction of BSA−peptide II bound to gold nanoparticles vs mol fraction added to solution. Mole fractions are calculated as moles of peptide II/total moles of peptides I and II.

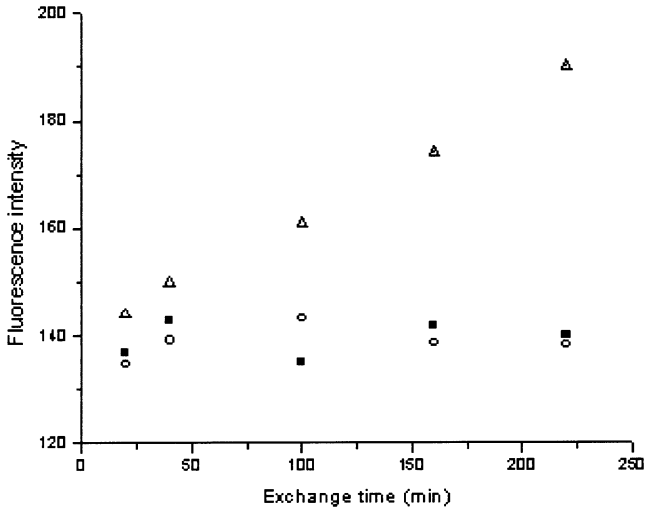

Figure 7. Fluorescence intensity of supernatant following exposure of RB−BSA−gold particle complexes to solutions containing native BSA (triangles), glutathione (circles), and phosphate buffer (squares).

samples incubated in the absence or presence of glutathione, even after 240 min (Figure 7). These data indicate that glutathione in solution at concentrations found inside cells does not displace BSA from gold nanoparticles. Exchange experiments in which RB−BSA was bound to gold particles and native BSA was placed in solution indicated that native BSA does remove RB−BSA from the nanoparticle surface. The slope of the plot in Figure 7 revealed an exchange rate of ∼2 BSA molecules every ∼12 min.

DISCUSSION

Bovine serum albumin is widely used in cytochemical studies as a molecular scaffold for the conjugation of fluorescent markers, peptides, and protein fragments. However, a description of the structures and yields for conjugation steps has not yet been fully elucidated. In this study, we have employed multiple methods (phosphorescence, fluorescence) to corroborate the yield of the bioconjugate coupling and adsorption onto gold nanoparticles.

Preparation of labeled BSA involves coupling by the heterobifunctional linker MBS. The *N*-hydroxy succinimide ester is attacked by nucleophilic lysines in and on BSA. There are a total of 59 lysine residues on BSA, up to 34 of which may react with the NHS ester of MBS. However, there is no X-ray crystal structure available for BSA, and therefore, the location and environment of the lysine residues is not known precisely. To overcome this limitation, we have used homology modeling to obtain a structure for BSA using its high sequence homology with human serum albumin (HSA), whose X-ray crystal structure is known (PDB accession number 1BMO) (Figure 8). Based on an alignment with the sequence the homology was 72% between the two sequences. There is an overhang of 28 residues on C-terminal BSA sequence that is not found in HSA. Ignoring this C-terminal sequence that contains 2 lysines, the homology model indicates

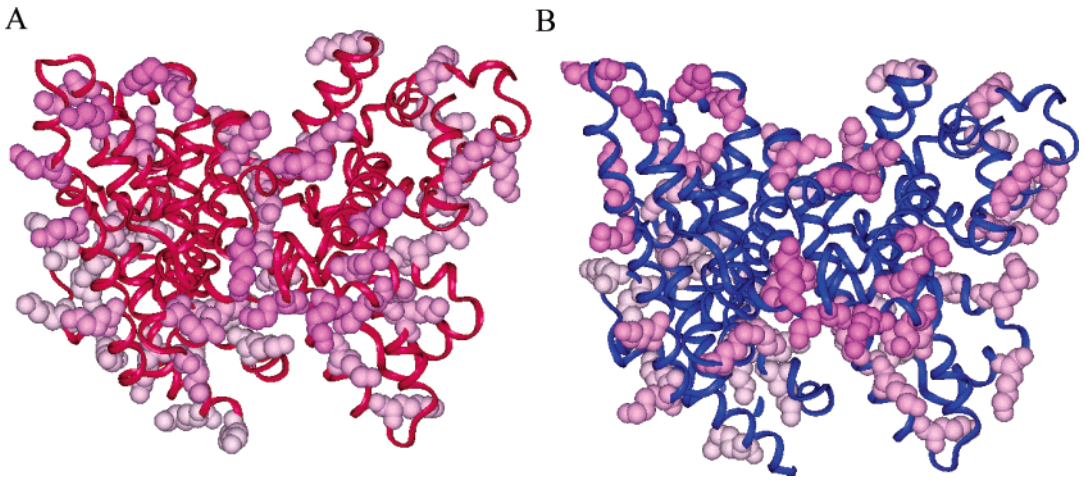

Figure 8. (A) 1BMO X-ray structure for human serum albumin. (B) Homology model for BSA. Lysines are shown in pink.

that there are 28 lysine residues on the surface of BSA and 30 more that are partially buried. There were essentially no lysines in the interior of the protein. Our binding isotherm for MBS has a maximum of 34 MBS molecules per BSA, which suggests that ~6 MBS ligands are at least partially buried and likely unavailable for further conjugation to thiol ligands (e.g., peptides). Of the remaining 28 surface-exposed MBS ligands, only 10 were found to react with incoming thiols, for a yield of ~35%. A combination of sterics and MBS hydrolysis is a likely source of such low yields.

The flocculation assays of gold nanoparticle suspensions followed the expected trends from DLVO theory—sol stability decreased with increasing salt concentration. According to DLVO theory, the stability of a gold colloid is determined by the balance of forces between electrostatic repulsion of like-charged spheres and van der Waals attraction due to the large polarizability of gold.[25] In general, the addition of electrolytes to gold nanoparticles causes flocculation as a result of the shielding of the repulsive double-layer charges.[26] Proteins or polymers adsorbed to the particle surface or free in solution will also influence the stability of metal sols. Proteins adsorbed to the particle surface will stabilize the sol due simply to the large positive free energy input of protein desorption required prior to particle−particle fusion. Proteins (or other macromolecules) in solution can cause particle flocculation or stabilization.[27] Flocculation occurs whenever colloidal particles approach so closely that the free protein is excluded from the interparticle region. This is an entropic effect; the protein leaves the interparticle region in response to the loss of configurational entropy upon compression by the particles. Loss of protein between the particles leaves behind pure solvent molecules. A reduction in free energy is subsequently gained when the solvent also leaves the interparticle region to mix with the protein. This "depletion flocculation" will only occur by demixing protein chains and solvent in the interparticle region. In good solvents, demixing is thermodynamically unfavorable, and the free protein in solution will actually stabilize the sol by preventing close approach of two particles (depletion stabilization).[27]

Both the flocculation assays and CFC tests showed that peptide-modified proteins stabilize gold sols better than the corresponding native protein. The comparison of uncentrifuged and centrifuged samples in Table 2 further indicates that protein concentrations in excess of those required for monolayer formation afford increased stability. The relatively large structures of BSA−peptide conjugates result in higher steric stabilization, which correspond to lower amounts of stabilizer required by gold particles and higher CFC values than that of native BSA. The fact that a large excess of BSA is required to fully stabilize the colloidal dispersions and that removal of the excess BSA results in dramatically decreased stability indicates that depletion mechanisms play an important role in the stabilization of colloidal gold−BSA systems.[27] The adsorption isotherms of BSA and BSA−peptide conjugates differed considerably (Figure 5). The isotherm of RB−BSA was the closest to the classic Langmuir type, which describes the formation of a monolayer on the surface. We do note, however, that the plateau of this isotherm is not totally flat, suggesting a small percentage of loosely bound proteins might exist. In contrast to RB−BSA, the isotherms of BSA−peptide conjugates revealed highly linear regimes, suggesting nonspecific binding occurs to a much larger degree compared to RB−BSA. The reason for the observed difference in binding between RB−BSA and the peptide-modified BSA is not known at this time.

A surface coverage of 160 ± 8 BSA/gold nanoparticle determined for $[Ru(bipy)_2bipy\text{-}C_6H_{12}\text{-}SH]^{2+}$-lableled BSA by TCSPC (Figure 4) agrees with the result of rhodamine B isothiocyanate−BSA determined by fluorescence spectroscopy (Figure 5A). TCSPC has proven to be a powerful technique for observing the microenvironment of phosphorescent probe molecules. The emission of $[Ru(bipy)_2bipy\text{-}C_6H_{12}\text{-}S]^{2+}$ is partially quenched on the gold surfaces present in the colloidal suspensions. This is evident in the shortening of the lifetime in the kinetic traces in Figure 4 when $[Ru(bipy)_2bipy\text{-}C_6H_{12}\text{-}S]^{2+}$ molecules adsorb to gold nanoparticles. Based on the comparison to a standard of known quantum yield, the relative quantum yields and lifetimes of the free and bound $[Ru(bipy)_2bipy\text{-}C_6H_{12}\text{-}S]^{2+}$−BSA can be determined. These yields permit an accurate determination of the number of $[Ru(bipy)_2bipy\text{-}C_6H_{12}\text{-}S]^{2+}$−BSA molecules on the surface of a nanoparticle. Interestingly, earlier radiolabeling studies

(25) Adamson, A. W. *Physical Chemistry of Surfaces*, 5th ed.; John Wiley & Sons: New York, 1990.
(26) Niemeyer, C. M. *Angew. Chem., Int. Ed.* **2001**, *40*, 4128−4158.
(27) Hunter, R. J. *Foundations of Colloid Science*; Oxford University Press Inc.: New York, 1991.

done on 15-nm citrate-capped gold nanoparticles[17,28] concluded that 39 native BSA molecules are adsorbed at monolayer coverage. The corresponding monolayer coverage for 20-nm gold nanoparticles, taking only the relative surface areas into consideration, would be ~70 BSA/gold. The discrepancy with the number observed above (160 ± 8) could be due to electrostatic differences that arise from the different labels on BSA, differences in crystallinity between the gold particles (i.e., surface area may not scale precisely with particle radius), or different solvent conditions. Another important difference between radiolabeling studies and TCSPC is that TCSPC is sensitive to the distance between the phosphorescent tag and the gold nanoparticle surface: only BSA bound to the nanoparticle surface is measured in TCSPC (e.g., monolayer adsorption). In this context, the 160 RB−BSA observed per gold nanoparticle signifies a dense mode of binding in which each BSA occupies ~7.5 nm^2 of the nanoparticle surface. Given that BSA is an oblong protein 10 nm long × 3 nm wide, the data suggest that BSA adsorbs onto gold nanoparticles end-on.

Irrespective of the detailed orientation of BSA binding to gold nanoparticles, the ease of the current methods compared to radiolabeling provides a ready experimental protocol to compare adsorption isotherms under a variety of solvent conditions, for peptide tags and bioconjugates and for various nanoparticle coatings. The combination of fluorescence quenching and lifetime measurements provides a simple one-pot assay for distinguishing between the bound and unbound fractions of BSA adsorbed on metal nanoparticles. Moreover, TCSPC should in principle be easily extended to most any fluorescent adsorbate.

(28) Baudhuin, P.; Van der Smissen, P.; Beauvois, S.; Courtoy, P. J. *Colloidal Gold: Principles, Methods, and Applications*; Academic Press: New York, 1989.

CONCLUSIONS

A primary goal of our research is to increase the stability of biomolecule−nanoparticle complexes in biologically relevant media (e.g., solutions of high ionic strength such as cell growth media and blood plasma). The studies presented here demonstrate that BSA can be an effective linker for peptide conjugation to gold nanoparticles. Particle coagulation or exchange of surface-bound BSA in the presence of electrolytes and thiol molecules found in biofluids is sufficiently slow that a nanoparticle−BSA complex can be used as a research tool in cellular imaging studies. In addition, we have demonstrated that two peptides with different cell-targeting properties partition onto nanoparticles with an average mole fraction that is not dramatically different from their mole fraction in solution. The observation of such partitioning is important to the development of multifunctional nanoparticles for studies in cell biology and medicine. Finally, the characterization of metal particle bioconjugates will be aided by the application of new tools that can monitor adsorption kinetics and ligand exchange mechanisms in real time. The work presented here suggests that time-correlated single photon counting spectroscopy is a useful tool for studying such processes.

ACKNOWLEDGMENT

The authors thank the David and Lucile Packard Foundation, The Arnold and Mabel Beckman Foundation, NSF DMR (9900073), NIH, and NSF-MDB (9874895) for support of this work.

Received for review May 29, 2003. Accepted August 21, 2003.

AC034578D